Arch. Metall. Mater., Vol. 61 (2016), No 2B, p. 1193–1200

DOI: 10.1515/amm-2016-0198

S. BŁACHA*#, M.ST. WĘGLOWSKI*, S. DYMEK**, M. KOPUŚCIAŃSKI**

MICROSTRUCTURAL CHARACTERIZATION AND MECHANICAL PROPERTIES OF ELECTRON BEAM WELDED JOINT OF HIGH STRENGTH STEEL GRADE S690QL

In the paper the results of metallographic examination and mechanical properties of electron beam welded joint of quenched and tempered steel grade S690QL are presented. Metallographic examination revealed that the concentrated electron beam significantly affect the changes of microstructure in the steel. Parent material as a delivered condition (quenched and tempered) had a bainitic-martensitic microstructure at hardness about 290 HV0.5. After welding, the microstructure of heat affected zone is composed mainly of martensite (in the vicinity of the fusion line) of hardness 420 HV0.5. It should be noted, however, that the microstructure of steel in the heat affected zone varies with the distance from the fusion line. The observed microstructural changes were in accordance with the CCT-S transformation diagram for the examined steel.

Keywords: electron beam welding, high strength quenched and tempered steel, microstructure

1. Introduction

In recent years, the manufacturing industry is focused on the application of high strength (HS) and ultra-high strength steels (UHS) that, simultaneously, exhibit low brittle to ductile transition temperature (BDTT). It is associated with the evolution of steel structures that are more complex, bigger and exposed to non-friendly environment. At the same time, the reduction of weight and production costs become an important issue due to the competition between steel manufacturers. Such steels are usually used in the quenched and tempered condition. The required BDTT is provided by the fine-grain microstructure. By selecting an appropriate chemical composition as well as the working conditions and heat treatment it is possible to obtain steels with yield strengths up to 1300 MPa [1].

The principal advantage of these steels is a good combination of strength and toughness, higher strength/weight ratio and accepted formability. However, their weldability is not sufficient for modern applications. The high strength steels are mainly applied in the construction of cranes, heavy duty trucks, mobile cranes and other highly loaded components [2]. They are also useful in an automobile industry [3-10]. Since the weldability remains the Achilles' heel of a broader application of these steels the emphasis is now put on the development of such a welding technology that only marginally reduces steel properties during welding. Also, the deeper understanding of phenomena occurring during welding that influence the microstructure, and thus properties, of the welded elements become an important issue in broader application of these steels.

The S690Q steel belongs to this group of steels – nowadays it gains increasing popularity in industry. It has higher strength than S355 or S460 grade that are used in similar applications, however, its weldability is worse because of the higher content of alloying elements like Mn and by a high tendency of thicker welded joints to cold cracking [11]. It has been already shown that producing high quality joints requires rigorous welding conditions that comprise such factors like the amount of heat input to the joint, preheating temperature, type of filler metal as well as specific welding conditions [12]. The inappropriate conditions may sensitize the thicker joints to cold cracking [11]. Numerous investigations were performed in order to understand the behavior of the HS and UHS steels during welding. It was shown [13] that the planning of the welding technology for a quenched and tempered high strength steel an extremely "narrow window" of parameters should be defined. The welding technology can be successfully planned on the basis of the optimal $t_{8/5}$ cooling time range. The influence of the $t_{8/5}$ time on hardness, impact toughness and microstructure was discussed in Ref. [14]. The results show that the impact toughness and hardness decrease with the increase of the $t_{8/5}$ under condition of a single thermal cycle in the simulated HAZ. The increase of cooling time to 300 s produced the microstructure that was composed of ferrite and bainite mixture. The $t_{8/5}$ longer than 60 s resulted in lower hardness and the lower risk of cold cracking in the HAZ.

* INSTITUTE OF WELDING, DEPARTMENT OF THE TESTING OF MATERIALS WELDABILITY AND WELDED CONSTRUCTION, 16-18 BŁOGOSŁAWIONEGO CZESŁAWA STR., 44-100 GLIWICE, POLAND
** AGH UNIVERSITY OF SCIENCE AND TECHNOLOGY, FACULTY OF METAL ENGINEERING AND INDUSTRIAL COMPUTER SCIENCE, 66 CZARNOWIEJSKA STR., 30-054 KRAKOW, POLAND
# Corresponding author: sylwester.blacha@is.gliwice.pl

It was also demonstrated that the pre-heating procedure has to be applied prior to welding, particularly in the case of structures with a high degree of restraint of connected elements and being welded using additional material of high strength and high hydrogen content [15]. The other investigations revealed that the welded joints of high strength steel (yield strength up to 960 MPa) are susceptible to hydrogen cracking in both, heat affected and fused zones [16,17].

The cold cracking process as well as the proper preheating temperature in MAG welding of UHS steel was investigated in Ref. [2]. A Tekken cold cracking test was used to assess the weldability of the UHS steel at two different heat inputs and at different preheating temperatures from the range of 20 to 200°C. The experimental results showed that the heat input and preheating temperature decided on the tendency to cold cracking. The optimal preheating temperature, in this research, was about 100°C. However, the results revealed that the analytical formulas used for calculating of the preheating temperature were not useful for this kind of steel.

The interaction between heat control (interpass temperature and heat input) and both local and global stresses in HS steel welds were also studied [18]. The investigations were focused on mechanical and microstructural properties an UHS steel (S960Q) in quenched and temper conditions. It was that shown that, for MAG welds, the best mechanical properties were achieved when cooling time was in the range 6-10 s for at the lowest possible linear energy (500-700 J/mm). Another research provided evidences that excellent toughness in welded steels could be obtained when microstructure was composed almost entirely of lower bainite with negligible amount of retained austenite [19].

All of these investigations indicate that the development of a new welding process for high strength steels is an important issue in improving the weld quality. In this regard, electron beam welding (EBW) can be one of the prospective technology. Electron beam welding utilizes the energy from a fast-moving beam of electrons focused on the base material. The electrons strike the metal surface, giving up their kinetic energy almost completely in the form of heat. Welds are made in a vacuum, which practically eliminates contamination of the weld material by the gases left in the vacuum chamber. Welds produced by this process are coalesced from vacuum-melted material, which eliminates the usual fusion weld contaminants caused by water vapor, oxygen, nitrogen, hydrogen, and slag [20]. The EBW gives additional advantages over fusion welding – neither filler metal nor shielding gasses are involved in the welding process. It is well documented that the non-vacuum electron beam welding of high strength steel can significantly reduce, compared with arc welding processes, the number of passes, the welding time, and the filler consumption [21]. Simultaneously, the short thermal cycle during electron bean welding does not change substantially of the bainitic-martensitic microstructure of the welded steels. In addition, the EBW substantially increases the welding speed [22].

In the present paper the microstructure and mechanical properties of electron beam welded joints, made of high strength S690QL steel in quenched and tempered condition, were examined. The emphasis was put on microstructural changes in the steel subjected to the influence of a concentrated beam of electrons.

2. Experimental procedure

The investigation was carried out on test joints of the S690QL steel grade. The chemical composition and nominal mechanical properties (acc. to PN-EN 10025-6 [23]) of the steel S690QL are given in Tables 1 and 2, respectively.

TABLE 1

Chemical composition of the S690QL steel [23]

Chemical composition [%] wt.						
C	**Si**	**Mn**	**B**	**Nb**	**Cr**	**V**
0.22	0.86	1.80	0.006	0.07	1.60	0.14
Cu	Ti	Mo	Ni	N	P	S
0.55	0.07	0.74	2.10	0.016	0.025	0.012

TABLE 2

Mechanical properties of the S690QL steel [23]

	R_e	R_m	A_5	**HV0.05**
S690QL	Min 690	770-940	Min 14	290

The welded joint, in a butt configuration, was produced by an Electron Beam Welding Machine, model XW150:30/756 (producer: Cambridge Vacuum Engineering Ltd, United Kingdom) (Fig. 1) located at Institute of Welding in Gliwice.

Fig. 1. The electron beam machine for welding and surface modification model XW150:30/756

Prior to welding the preliminary assessment of the changes in microstructure produced by the electron beam of diverse energy was performed. To complete this task, the 10 mm thick steel blanks were electron beam treated at the following parameters:

– accelerating voltage U = 150 kV,

– beam current I = 3 mA, 5 mA, 10 mA, 12 mA, 16 mA, 18 mA and 20 mA,
– speed of welding 500 mm/min,
– focal distance 760 mA.

The applied beam currents correspond to the following values of linear welding energy (kJ/cm): 0.56, 0.9, 1.9, 2.3, 2.9, 3.2, 3.6.

The linear energy of 2.8 kJ/cm was selected as the most appropriate for the welding. The welding was performed without a filler metal and without preheating. The microstructural examinations of the steel in the as-received and post-welded conditions were carried out by means of light and scanning electron microscopy on sections perpendicular to the direction of welding. Prior to the observation the samples were etched by the 2% Nital reagent. Additionally, the selected samples were etched by a solution of 2 g $CuCl_2$ + 40 ml C_2H_2OH + 40 ml HCl in order to reveal bainite in the polarized light.

For the comparison purposes the traditional metal active gas (MAG) welding of the same steel (S690QL) pieces was also performed. The welding parameters in this case were: welding speed 350 mm/min and the linear energy 10.2 kJ/cm.

The Vickers microhardness (HV 0.05) and hardness (HV10) measurements across the HAZ and base metal were carried out on the metallographic samples. The microhardness measurements were performed on the Prüftechnik KB 50 automatic hardness tester.

3. Results and discussion

The microstructure of the S690QL steel in the as-received condition was composed of martensite and bainite (Fig. 2).

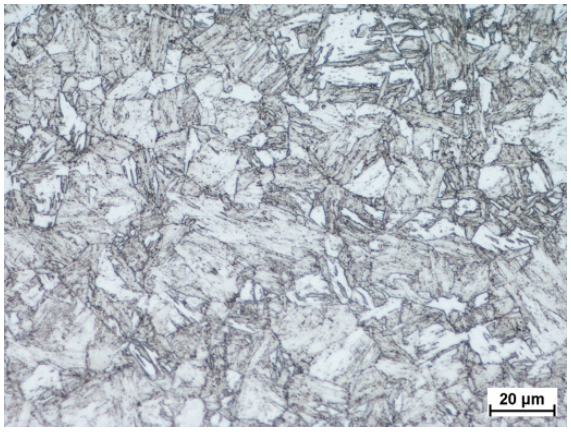

Fig. 2. The microstructure of S690QL steel after heat treatment, light microscopy

The concentrated electron beam altered significantly this microstructure. The light microscopy metallographic examination revealed different zones in the interaction volume that were closely related to the temperature and cooling rate. The heating and cooling rates of the individual regions, due to the high energy of beam and small volume of interaction, are relatively high, but different in the particular zones. Therefore, it can be distinguished the melted zone in which the material from the liquid transforms to the solid state and is subsequently subjected to quenching. Thus, the martensitic-bainitic microstructure dominates in this area. The bainitic microstructure was revealed in polarized light after specific etching that turned bainitic areas into blue color (Fig. 3).

a)

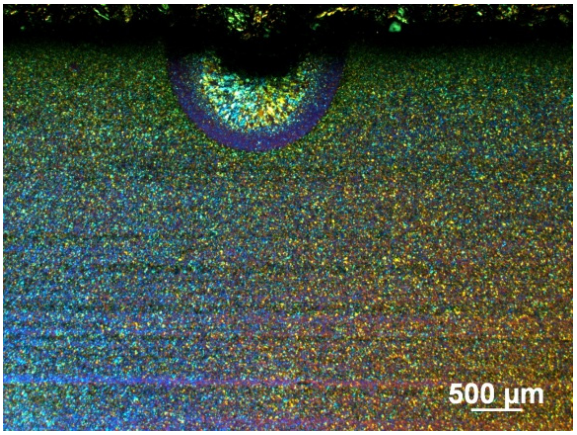

b)

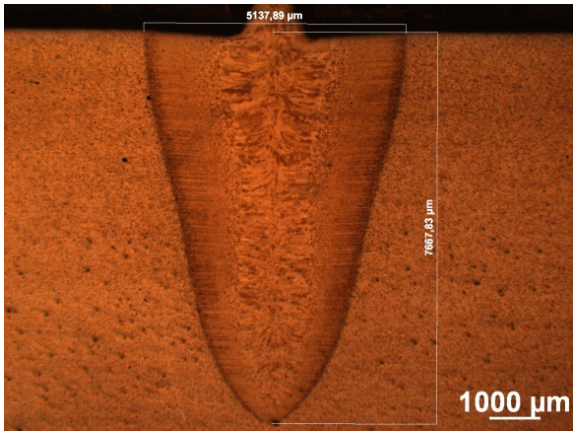

Fig. 3. Specimens for established of microstructure at different beam current, a) I = 3 mA, b) I = 18 mA

The heat affected zone (HAZ) also exhibited very complex microstructure that reflected the exposition to different temperatures and different cooling rates. In general, a few types of microstructures can be distinguished within the HAZ, however, there are no well-defined boundaries between areas with different microstructures. Instead, one type of microstructure change into another in a rather smooth manner. The region adjacent to the melted zone is characterized by a coarse grain size. It is likely a region that was heated to temperatures well above 1000°C and then quenched. Next to it is a fine-grained area that was heated up to a temperature lower than 1000°C but higher than the transformation temperature Ac3. The following, much narrower, zone contains a mixture of ferrite and bainite. Such a microstructure suggests that this region was heated up to a temperature range between Ac1 and Ac3.

The width of remelting areas (measured at the weld face) and the penetration depth are largely dependent on the beam energy (Fig. 4). The results of the width and depth measurements

are presented in Table 3. The value of the depth to width ratio, that increases with increasing of beam energy (beam current), is also shown in the Table 3. The broadness of particular areas in the HAZ with different microstructure was also evaluated (Fig. 5). All measurements were taken near the mid-depth region of the interaction volume. The results are shown in Table 4. The measurements are not precise due to the inevitably arbitrary determination of the boundaries between particular regions. Thus, the values in the Table 4 should be considered as approximations. However, the general trend showing the dependence of the microstructure on the electron beam energy can be demonstrated.

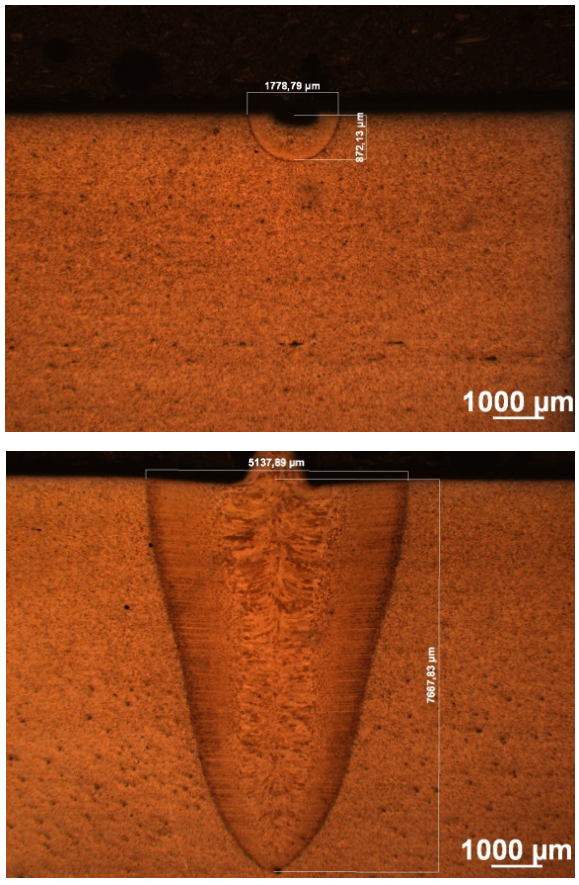

Fig. 4. Specimens for measurement of width of face of weld at different beam current, a) I = 3 mA, b) I = 20 mA

TABLE 3

The relationship between beam current and penetration depth and width of face weld, steel S690QL (numerical values are given in microns)

Beam current [mA]	Penetration depth	Width	Penetration / width
3	872	1778	0,49
5	1511	2530	0,60
10	3091	3946	0,78
12	3963	4179	0,95
16	6312	4576	1,38
18	7296	4775	1,53
20	7667	5137	1,49

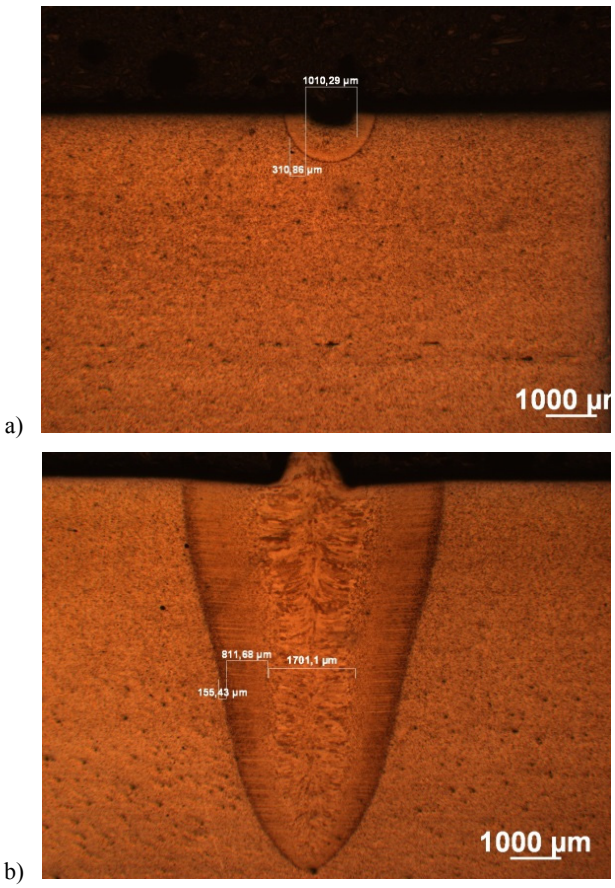

Fig. 5. Specimens for measurement of zones at different beam current, a) I = 3 mA, b) I = 20 mA

TABLE 4

The relationship between beam current and width of each zone, steel S690QL (numerical values are given in microns)

Beam current [mA]	Melting zone	Grain refirement zone	Ac1 – Ac3
3	1010	310	–
5	1325	389	44
10	2141	579	95
12	1891	725	108
16	1416	742	173
18	1400	682	130
20	1700	811	155

The preliminary research on the interaction of the electron beam with the S690QL steel made it possible to select process parameters for welding. The macrostructure of the EB weldment produced at the 3.8 kJ/cm linear energy and 500 mm/min welding speed is shown in (Fig. 6). For comparison, (Fig. 7) shows the macrostructure of the MAG welded joint.

The weldedment made by the electron beam is characterized by the high ratio of the penetration depth of to the width at the weld face. In this test case, the penetration depth was 10 mm (thickness of the sheet) and weld width – 3.8 mm. It is worth to note, that the heat affected zone was very narrow – it did not exceed 1.3 mm. On the other hand, the width of the joint produced by the traditional arc welding method (MAG) was about 23 mm

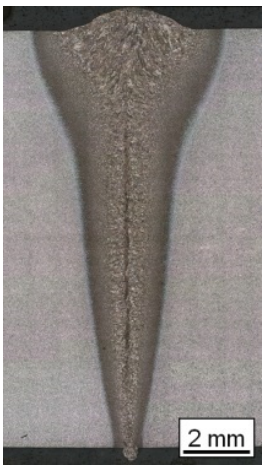

Fig. 6. Macrostructure of electron beam welded joints made of steel S690QL, one run

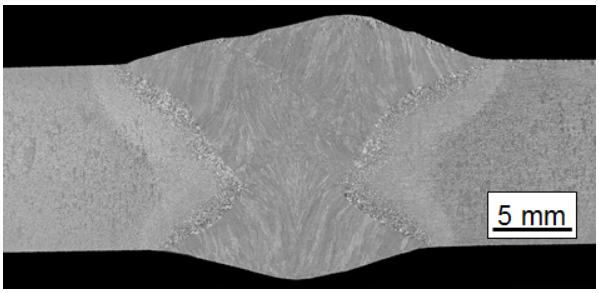

Fig. 7. Macrostructure of MAG welded joints made of steel S690QL, 12 runs

and the width HAZ about 3.6 mm (Fig. 7). The narrow electron beam weld is associated with a high power density and high kinetic energy of electron beam striking the welded material. The concentrated welding beam supplies a relatively small amount of energy to the weld vicinity. Thus, the energy efficiency of the process is high. The very high power density makes it possible to vaporize the material and produce a deep-penetrating keyhole and hence weld. With a very high power density in EBW, full-penetration keyholing is possible even in thick workpieces. Joints that require multiple-pass arc welding can be welded in a single pass at a high welding speed. Consequently, the total heat input per unit length of the weld is much lower than that in arc welding, resulting in a very narrow heat-affected zone and little distortion [Sindo Kou]. In the performed experiment (welding energy 3.8 kJ/cm, welding speed 500 mm/min) the cooling time in temperature interval from 800 to 500°C ($\Delta t_{8/5}$) can be less than 1 s [24]. On the other hand, in MAG electric arc welding (welding energy 10.2 kJ/cm, welding speed 350 mm/min) the heat energy is transferred to the base material through a pool of molten metal and the cooling time in this case is much longer ($\Delta t_{8/5}$ = 6 – 8 sec).

Despite the very small volume of the HAZ in the electron beam welded material, its microstructure is not a uniform. Several zones can be distinguished that differ in terms of morphology and the level of hardness. Figure 8 shows the microhardness profile (HV0.01) in the presented area. The results of supplemental hardness measurements (HV10), along with a schematic drawing of testing point placements, are also presented in Table 5.

The hardness values were lower than 450 HV10 – the permissible hardness level for qualifying welding technology according to the ISO 15614-11 specifications [25].

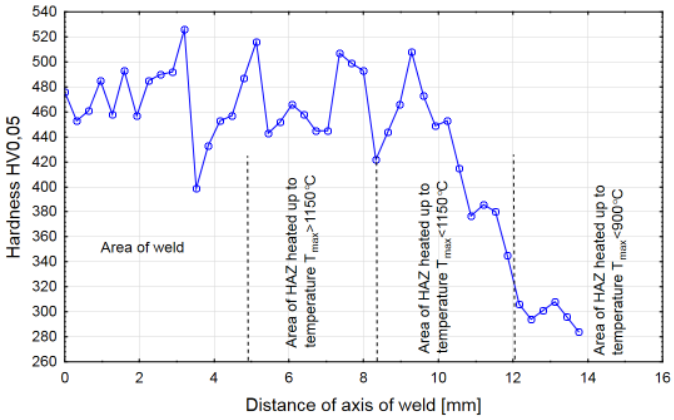

Fig. 8. The hardness distribution in the electron beam welded joint

TABLE 5

Results of hardness tests for electron beam welded joints, HV10

	1	2	3	4	5	6	7	8	9	10	11	12	13	14	15
Line A	267	270	268	411	422	429	407	419	431	415	421	424	274	275	272
Line B	272	269	274	422	431	434	435	426	430	439	430	445	275	278	274

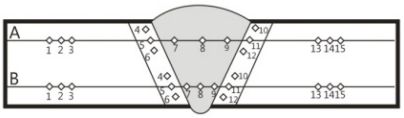

Figure 9 shows the changes in microstructure across the weld (in approximately mid-thickness of the joined plates) from the base material to the weld center. The microstructures of the individual regions of the electron beam welded joint observed in a light microscope at higher magnifications are shown in Figures 10 to 14. The observed differences in microstructure correspond to the data presented on the continuous cooling transformation (CCT) graph created for a similar grade of steel subjected to fast thermal cycles (Fig. 15).

The graph was constructed for a high heating rate about 6000°K/s that is consistent with rates occurring during EBW. In contrast, the typical austenite transformation graphs for weld-

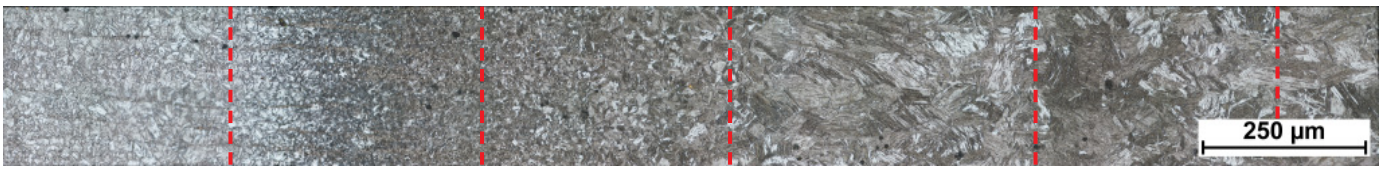

Fig. 9. The microstructure of a electron beam welded joint of steel S690QL with the selected characteristic areas: a) the parent material (Fig. 2), b) the area HAZ heated to a temperature between Ac1 Ac3 – (700 ≤ Tmax < 900°C) (Fig. 10), c) the area of fine-grained heated to a temperature above Ac3 (900 ≤ Tmax < 1150°C) (Fig. 11), d) the area of the structure SWC coarse (Tmax ≥ 1150°C) (Fig. 12), e) zone remelting (Fig. 13), f) axis of the weld (Fig. 14)

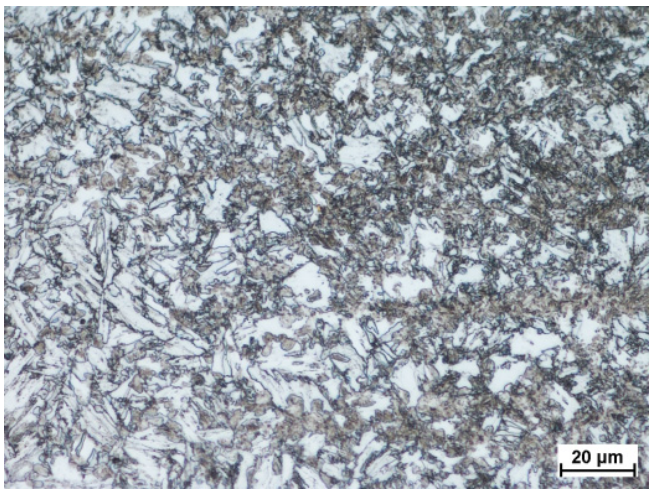

Fig. 10. Microstructure of the HAZ area heated up to a temperature between Ac1 Ac3 – (700 ≤ Tmax < 900°C), the area partially tempered 298 HV0.05 (region A, Fig. 9)

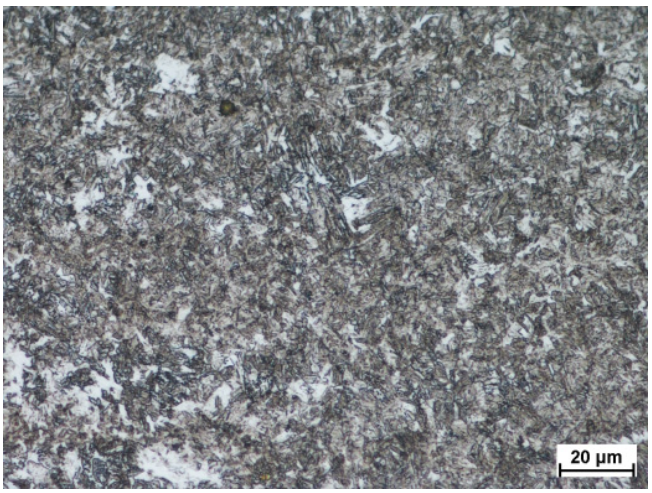

Fig. 11. The microstructure HAZ area heated to a temperature above Ac3 (900 ≤ Tmax < 1150°C), the area partially tempered, 380 HV0.05 (left side), 469 HV0.05 (right side), (area b , Fig. 9)

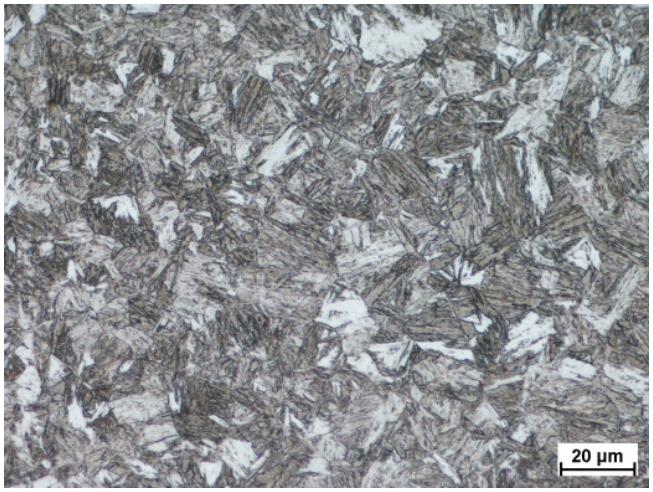

Fig. 12. The microstructure of HAZ area heated to temperature Tmax ≥ 1150°C, an area fully tempered, 451 HV0.05 (area c, Fig. 9)

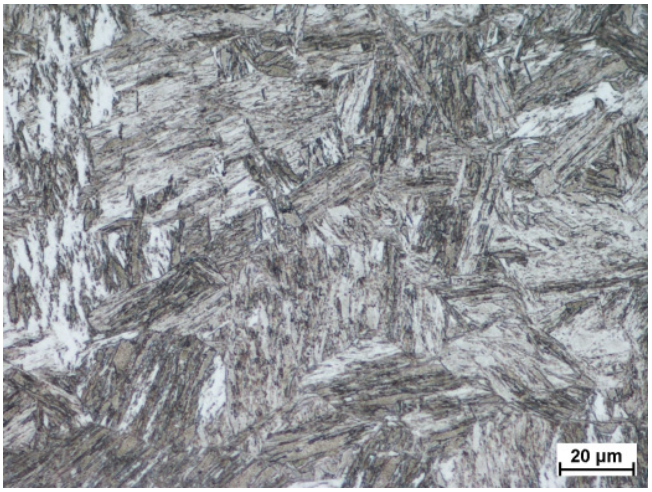

Fig. 13. The microstructure of melted zone area, 485 HV0.05 (area d, Fig. 9)

ing conditions are determined for the heating rate of 200°K/s. The typical martensitic microstructure with the hardness of 451 HV0.05 was observed near the fusion line (Fig. 8). This type of microstructure was formed due to quenching (short cooling time $\Delta t_{8/5}$) of the weld material from high temperature. It also results from the CCT diagram that for longer cooling times $\Delta t_{8/5}$ the microstructure is composed of martensite and bainite. This is the case in the HAZ portion located farther from the fusion line (Figs. 10-11). When the distance from the fusion line increases, the temperature gradient is lower, the rate of heat dissipation is smaller. Thus, the time $\Delta t_{8/5}$ become longer that results in decreasing the hardness below 450 HV. The data in (Fig. 15) shows that at high heating rate of the SQ690QL steel and at fast cooling down ($\Delta t_{8/5}$ lower than 2s) the hardness of

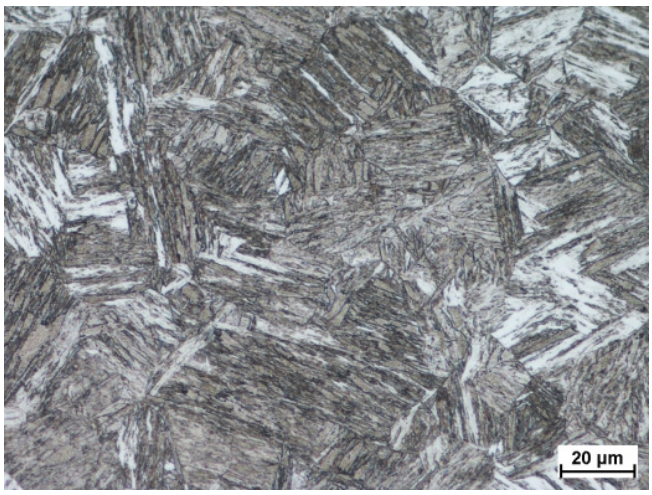

Fig. 14. The microstructure of the weld area – axis 468 HV0.05, light microscopy (area e, Fig. 9)

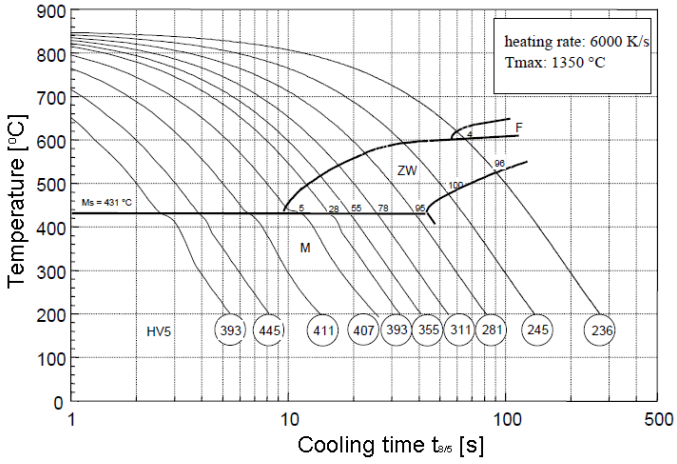

Fig. 15. CCT diagram for S690QL steel [26]

the steel is smaller than the hardness resulted from slower cooling ($\Delta t_{8/5}$ 3 seconds). A similar phenomenon is observed in the EBW joint examined in the present study. Near the fusion line (short cooling times $\Delta t_{8/5}$) the hardness is reduced to a value of 400 HV, and at a greater distance from the weld line the hardness increases to the value of 520 HV. Such a phenomenon is not observed in the arc welded joints where the heating rate is much lower than 200°K/s. Therefore, it is believed that at very rapid thermal cycles the level of austenite homogenization is small and the growth of austenite grains is suppressed. Unfortunately, there is no possibility of practical verification of this assessment for the EBW conditions. However, it is apparent that these fast thermal cycles have a significant impact on the microstructure and properties of the welded joint.

4. Conclusions

Based on the metallographic examination and hardness tests of the electron beam welded joint of steel S690QL the following conclusions can be formulated:

1. The width of remelted areas and penetration depths are largely dependent on the beam energy.
2. The joint made by EBW is 6 times narrower than the joint produced by MAG; the width of the heat affected zone is also narrower.
3. The microstructure of heat affected zone depends on the distance from the fusion line – it is composed of martensite near the fusion line and bainite in the very vicinity of the base material.
4. The microhardness in the HAZ exceeds the value of 520 HV0.05 near the fusion line and decreases to 280 HV0.05 in the vicinity of the base material, however, the hardness measured at the load 10 kg (according to the ISO 15614-11 standard – specification and qualification of welding procedures for metallic materials) is lower than 450 HV10, i.e. on the permissible level.
5. Near the fusion line (short cooling times $\Delta t_{8/5}$) the hardness is reduced to 400 HV, however, at a greater distance from the weld line the increase of hardness to 520 HV was observed.

Acknowledgments

The authors would like to thank The Polish Ministry of Science and Higher Education for financing the research. The research was performed within the framework of the statutory activity of the Instytut Spawalnictwa.

REFERENCES

[1] M.St. Węglowski, Modern toughened steels – their properties and advantages, Biuletyn Instytutu Spawalnictwa **56**(4), 32-38, 41 (2012).

[2] M.St. Węglowski, M. Zeman, Prevention of cold cracking in ultra-high strength steel Weldox 1300, Archives of Civil and Mechanical Engineering **14**(3), 417-424 (2014).

[3] A.A. Grajcar, Thermodynamic analysis of precipitation processes in Nb-Ti-microalloyed Si-Al TRIP steel, Journal of Thermal Analysis and Calorimetry **118**, 1011-1020 (2014).

[4] A. Grajcar, M. Rozanski, S. Stano, et al., Microstructure characterization of laser-welded Nb-microalloyed silicon-aluminum TRIP steel, Journal of Materials Engineering and Performance **23**, 3400-3406 (2014).

[5] M.St. Węglowski, K. Krasnowski, K. Kwieciński, R. Jachym, The characteristics of Nd:YAG laser welded joints of dual phase steel, Archives of Civil and Mechanical Engineering **9**, 85-97 (2009).

[6] A. Grajcar, M. Rozanski, S. Stano, et al., Effect of heat input on microstructure and hardness distribution of laser welded Si-Al TRIP-type steel, Advances in Materials Science and Engineering, Article Number: 658947 (2014).

[7] T. Wegrzyn, S.Wieszala, Significant alloy elements in welded steel structures of car body, Archives of Metallurgy and Materials **57**, 45-52 (2012).

[8] A. Grajcar, W. Zalecki, et al., Dilatometric study of phase transformations in advanced high-strength bainitic steel, Journal of Thermal Analysis and Calorimetry **118**, 739-748 (2014).

[9] A. Grajcar, Microstructure evolution of advanced high-strength TRIP-aided bainitic steel, Materiali in Tehnologije **49**, 715-720 (2015).

[10] M.St. Węglowski, S. Stano, G. Michta, W. Osuch, Structural characterization of Nd:YAG laser welded joint of dual phase steel, Archives of Metallurgy and Materials **55**, 211-220 (2010).

[11] N. Enzinger, H. Cerjak, Characterisation of cracks in high strength steel weldments, Welding in the World **51**(11-12), 29-33 (2007).

[12] W. Vanovsek, C. Bernhard, M. Fiedler, R. Schnitzer, Effect of titanium on the solidification and postsolidification microstructure of high-strength steel welds. Weld World **57**, 665-674 (2013).

[13] M. Gaspar, A. Balogh, GMAW experiments for advanced (Q+T) high strength steels. Production Processes and Systems **6**(1), 9-24 (2013).

[14] M.St. Węglowski, M. Zeman, M. Łomozik, Weldability of toughened steels with the yield strength over 1000 MPa, Biuletyn Instytutu Spawalnictwa **56**, 202-206 (2012).

[15] M.St. Węglowski, M. Zeman and M. Łomozik, Physical Simulation of Weldability of Weldox 1300 Steel, Materials Science Forum **762**, 551-551 (2013).

[16] M. Opiela, Hydrogen embrittlement of welded joints for the heat--treatable XABO 960 steel heavy plates, Journal of Achievements in Materials and Manufacturing Engineering **38**, 41-48 (2010).

[17] M. Lachowicz, W. Nosko, Welding of structural steel Weldox 700, Welding Technology Review **82**(1), 13-18 (2010).

[18] D. Schroepfer, T. Kannengiesser, Correlating welding reaction stresses and weld process conditions for high-strength steel S960QL, Weld World **58**, 423-432 (2014).

[19] H. Sumi, K. Oi, K. Yasuda, Effect of chemical composition on microstructure and mechanical properties of laser weld metal of high-tensile-strength steel, Welding in the World **59**, 173-178 (2015).

[20] M.St. Weglowski, S. Błacha, A. Phillips, Electron beam welding – Techniques and Trends – Review. Vacuum **130**, 72-92 (2016).

[21] T. Hassel, R. Konya, M. Collmann, P. Schaumann, S. Priebe, T.A. Deißer, A. Beniyash, N. Murray, Fr.W. Bach, Economical joining of tubular steel towers for wind turbines employing non-vacuum electron beam welding for high-strength steels in comparison with submerged arc welding, Welding in the World **57**, 551-559 (2013).

[22] Fr.W. Bach, A. Beniyash, K. Lau, R. Konya, Nonvacuum electron beam welding of structural steels; the Paton welding journal **5**, 22-26 (2009).

[23] PN-EN 10025-6:2009, Hot rolled products of structural steels – Part 6: Technical delivery conditions for flat products of high yield strength structural steels in the quenched and tempered condition.

[24] H. Schultz, Electron beam welding. Abington Publishing, Cambridge, Great Britain, 1993.

[25] PN-EN ISO 15614-11:2005, Specification and qualification of welding procedures for metallic materials. Welding procedure test. Part 11: Electron and laser beam welding.

[26] P. Seyffarth, R. Schmidt, W.F. Demtschenko, U. Jasnau, Simulation of microstructure – transformation – kinetics of unalloyed constructional steel in case of fast thermal cycles. Proceedings of the 3rd LANE 2001, Meisenbach Verlag, Bamberg, (2001).